Nanotechnology **19** (2008) 155703 (11pp) doi:10.1088/0957-4484/19/15/155703

A metric for characterizing the bistability of molecular quantum-dot cellular automata

Yuhui Lu and Craig S Lent

Department of Electrical Engineering, University of Notre Dame, Notre Dame, IN 46556, USA

E-mail: lent@nd.edu

Received 8 October 2007, in final form 24 January 2008
Published 12 March 2008
Online at stacks.iop.org/Nano/19/155703

Abstract

Much of molecular electronics involves trying to use molecules as (a) wires, (b) diodes or (c) field-effect transistors. In each case the criterion for determining good performance is well known: for wires it is conductance, for diodes it is conductance asymmetry, while for transistors it is high transconductance. Candidate molecules can be screened in terms of these criteria by calculating molecular conductivity in forward and reverse directions, and in the presence of a gating field. Hence so much theoretical work has focused on understanding molecular conductance. In contrast a molecule used as a quantum-dot cellular automata (QCA) cell conducts no current at all. The keys to QCA functionality are (a) charge localization, (b) bistable charge switching within the cell and (c) electric field coupling between one molecular cell and its neighbor. The combination of these effects can be examined using the cell–cell response function which relates the polarization of one cell to the induced polarization of a neighboring cell. The response function can be obtained by calculating the molecular electronic structure with *ab initio* quantum chemistry techniques. We present an analysis of molecular QCA performance that can be applied to any candidate molecule. From the full quantum chemistry, all-electron *ab initio* calculations we extract parameters for a reduced-state model which reproduces the cell–cell response function very well. Techniques from electron transfer theory are used to derive analytical models of the response function and can be employed on molecules too large for full *ab initio* treatment. A metric is derived which characterizes molecular QCA performance the way transconductance characterizes transistor performance. This metric can be assessed from absorption measurements of the electron transfer band or quantum chemistry calculations of appropriate sophistication.

1. Introduction

Quantum-dot cellular automata [1–4] (QCA) offer a new paradigm for binary computing which may be better suited to molecular nanoelectronics than conventional current-based approaches. Molecular electronics typically focuses on forming current-carrying molecular wires, diodes and field-effect transistors. In the QCA scheme, in contrast, binary information is represented by the charge configuration of QCA cells. As figure 1 shows schematically, each QCA cell contains four quantum dots, which are simply sites electrons can occupy and on which charge is approximately quantized. Two mobile charges repel and so occupy antipodal sites of the cell, providing two stable charge configurations which encode a binary '0' or '1.' The Coulomb interaction between neighboring cells provides device–device coupling for information transfer. This cell–cell interaction is the basis of QCA device operation. No current flows from cell to cell.

QCA devices have been fabricated with dots formed by small aluminum islands in the Coulomb-blockade regime. Metal oxide tunnel junctions between dots provide the tunneling pathways. QCA logic gates, shift registers, wires, inverters and fan-outs have all been demonstrated in this material system [4, 5]. Because the charging energies of the metallic islands are still fairly small (compared with comparable molecular energies) metal-dot QCA devices can

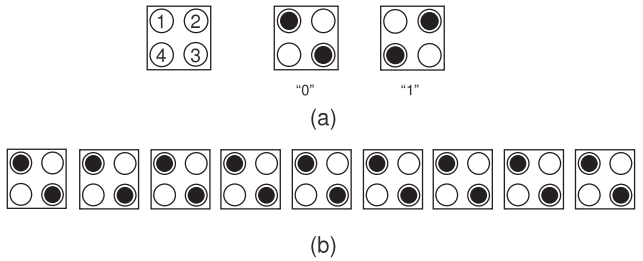

Figure 1. (a) Schematic of a QCA cell. The four dots are labeled 1, 2, 3 and 4. Binary information is encoded in the charge configuration. (b) A QCA wire.

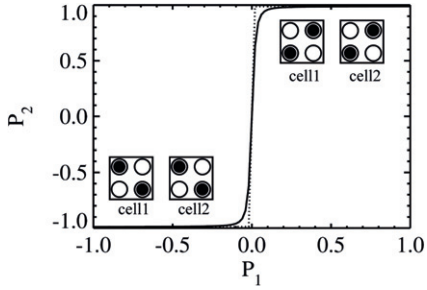

Figure 2. The QCA cell–cell response function. Cell 2 is driven by cell 1 via Coulomb interaction. P_1 and P_2 denote the polarization of cell 1 and cell 2.

only operate at cryogenic temperatures. They can be viewed as cryogenic prototypes of molecular devices. They provide proof-of-principle demonstrations of coupled single-electron operation of QCA circuits.

QCA devices can be shrunk to the molecular level [6, 7] so that single molecules act as QCA cells. Redox centers within the molecule serve as quantum dots, with tunneling paths provided by bridging ligands. There are several advantages to molecular QCA: first, molecules provide QCA cells of uniform size, overcoming the challenge of mass producing uniformly sized devices at the nanometer scale; second, the small size of molecules allows high device density [8] in the range of 10^{11}–10^{14} devices cm^{-2}; third, the Coulomb interaction between neighboring molecules is strong enough for molecular QCA to operate at room temperature [9]. There is also support for the possibility of molecular QCA device operation with ultra-low power dissipation [10] approaching the theoretical limits imposed by fundamental considerations.

Several candidate QCA molecules have been synthesized and experimentally characterized. Fehlner and coworkers [11–14] have explored mixed-valence complexes as QCA molecules. A measurement of the capacitance between the two redox centers of a double-dot molecule trans-$Ru(dppm)_2(C{\equiv}CFc)(NCCH_2CH_2NH_2)$ dication [11] attached to a Si substrate showed a switchable bistable charge configuration, the fundamental requirement of QCA molecules. A more complicated four-dot molecule has also been synthesized and isolated [12, 14]. Theoretical studies [9] have confirmed the bistable charge configuration in these molecules as well, and show further that the Coulomb interactions between neighboring molecules are strong enough to support bit operations at room temperature.

For conventional molecular electronics involving using molecules as wires, diodes or transistors, the desirable criteria for characterizing performance are well known: for wires it is high conductance, for diodes it is asymmetric conductance, while for transistors it is high transconductance. Candidate molecules can be screened in terms of these criteria by calculating molecular conductivity in forward and reverse directions, and in the presence of a gating field.

Different criteria, however, must be developed for assessing candidate QCA molecules, in which no current flows at all. The keys to QCA functionality are (a) charge localization, (b) bistable charge switching within the cell and (c) electric field coupling between one molecular cell and its neighbor. The combination of these effects which produce useful QCA behavior can be examined using the *cell–cell response function* which relates the charge configuration of one cell to the configuration induced in a neighboring cell.

The charge configuration of a QCA cell can be characterized by the cell polarization. For a four-dot QCA cell, the polarization is defined by

$$P = \frac{(\rho_1 + \rho_3) - (\rho_2 + \rho_4)}{\rho_1 + \rho_2 + \rho_3 + \rho_4}$$

where ρ_i is the charge on each quantum dot i as labeled in figure 1. To be used as a QCA cell, the polarization of one molecule must be coupled to the polarization of neighboring molecules. Consider the case of two nearby cells shown in the inset of figure 2. For any given polarization of cell 1, labeled P_1, a certain polarization P_2 will be induced in neighboring cell 2 via Coulomb interactions. The function $P_2(P_1)$, the induced polarization as a function of the neighboring polarization, is the cell–cell response function, shown in figure 2.

The cell–cell response function shown has two important features: (1) the polarization saturates near $P \approx \pm 1$ due to charge localization and bistability and (2) a small polarization in one cell induces a large polarization in its neighbor, a consequence of the Coulomb coupling between cells and the designed cell structure. The first feature allows the connection between cell polarization and a bit of information. For this four-dot cell we associate a state with $P \approx +1$ with a bit value of '1' and state with $P \approx -1$ with a bit value of '0'. The second feature gives the intrinsic signal restoration necessary to preserve digital logic levels from stage to stage.

Our goal here is to illuminate the relationship between molecular structure and QCA functionality in QCA-active molecules, so that we have a useful metric for evaluating candidate systems. The key features of molecular structure turn out to be geometric (the distance between redox centers) and electronic (the electron transfer matrix element). These we relate to QCA functionality as characterized by the cell–cell response function, and particularly the slope of the response function at the origin.

We present a simple model for calculating the cell–cell response function of a QCA candidate molecule by extracting key aspects of the structure—in particular with the electron transfer (ET) matrix element and the dot–dot distance

between redox centers. Our model is based on the two-state approximation (TSA) [15], in which the ET dynamics are accounted for by the two-component space (denoted as the donor–acceptor space) spanned by states in which the transferring electron is primarily localized at the donor and acceptor sites. A more detailed discussion of TSA can be found in [15]. We compare our model with fuller quantum chemistry calculations and deduce a simple metric for characterizing the requisite QCA bistability. We show how this metric can be evaluated from theory or experimental results.

It is important to note that many QCA candidate molecules are mixed-valence complexes which include transition metals [11–14]. Calculating the electronic structures of these molecules is challenging, particularly with regard to getting charge localization correct. Among quantum chemistry techniques, the Hartree–Fock (HF) method typically overestimates charge localization of a mixed-valence compound while density function theory (DFT) underestimates it [16–19]. A multiple reference self-consistent field (MCSCF) method [20] is needed to obtain an accurate electronic structure of a mixed-valence complex, making the full calculation extremely difficult and making simpler models that can capture the relevant physics attractive.

It is worth noting that, for QCA operation, the driving force of ET is the Coulomb interaction among neighboring molecules rather than the nuclear relaxation. Nuclear relaxation does play a very important role in ET and we have explored that effect in previous work [6]. Previous studies have shown that the consequence of nuclear relaxation is that charge localization is enhanced—the relaxation tends to deepen the potential well the electron is in. Considering the nuclear degrees of freedom fixed, is therefore a conservative approach. If a molecule shows QCA action with nuclear positions frozen, it will likely perform only better when nuclear relaxation is included. The exception to this is, of course, if the nuclear reorganization energy is larger than the Coulomb driving energy. In that case the charge will be stuck on one site.

It is also important to note that we do not aim here to study the time-dependent dynamics of QCA switching, but rather to develop tools for evaluating what makes a good QCA molecule. A dynamical treatment would go beyond ground state calculations and include thermal excitation effects and scattering mechanisms. Again, some work in this direction has been done [10].

The rest of this paper is organized as follows: in section 2 we present the theoretical background and derivation of our model. In section 3, we compare the energy diagram and cell–cell response functions calculated by our model for two simple molecules, with those calculated using *ab initio* techniques. We then use our model to predict response functions for mixed-valence diferrocenylpolyenes, which may serve as QCA candidate molecules. Finally, we present a brief conclusion in section 4.

2. Theory

A double-dot QCA cell can be modeled by a double well as shown in figure 3. Two quantum dots are represented by two

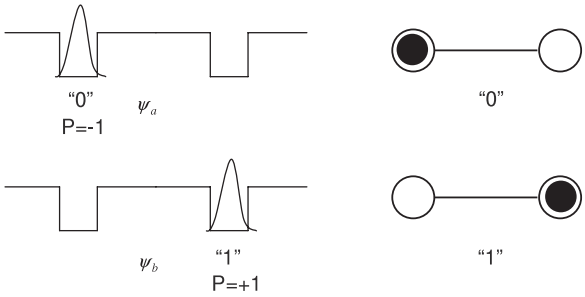

Figure 3. The scheme of the two-state model for a double-dot QCA cell. Two localized states are used to encode binary information.

quantum wells. The mobile charge localizes in either one of the two wells, encoding the cell's binary information. Note that the full four-dot cell shown in figure 1 can also be viewed as a pair of half-cells (with two dots each) in which the sign of the polarization alternates.

Under the two-state approximation, ET dynamics are described in a two-dimensional Hilbert space spanned by the two localized states shown in figure 3. Let ψ_a and ψ_b denote the wavefunctions of the '0' and '1' states. When the overlap integral $S_{ab} = \langle\psi_a\psi_b\rangle$ is neglected and the mixing coefficients are normalized ($c_a^2 + c_b^2 = 1$), the wavefunctions for the lower (ground state ψ_1, energy E_1) and upper (excited state ψ_2, energy E_2) adiabatic states are given by

$$\psi_1 = c_{a1}\psi_a + c_{b1}\psi_b \tag{1a}$$

$$\psi_2 = c_{a2}\psi_a + c_{b2}\psi_b. \tag{1b}$$

The energies of the adiabatic states are obtained by solving the secular equation for the two-state Hamiltonian:

$$\begin{vmatrix} H_{aa} - E & \gamma \\ \gamma & H_{bb} - E \end{vmatrix} = 0 \tag{2}$$

where H_{aa} and H_{bb} are the energies of the localized (diabatic) '0' and '1' states and given by

$$H_{aa} = \langle\psi_a|H|\psi_a\rangle \qquad H_{bb} = \langle\psi_b|H|\psi_b\rangle \tag{3}$$

and γ is the ET matrix element coupling the diabatic states:

$$\gamma = \langle\psi_a|H|\psi_b\rangle. \tag{4a}$$

The ET matrix element can also be related to the adiabatic energies:

$$\gamma = \frac{E_2 - E_1}{2}. \tag{4b}$$

Under the two-state approximation equations (4a) and (4b) are equivalent. Once the eigenenergies E_1 and E_2 of the adiabatic states are determined, the coefficients c_a and c_b can be obtained for the ground state and the excited state by solving the equation

$$\begin{bmatrix} H_{aa} & \gamma \\ \gamma & H_{bb} \end{bmatrix} \begin{bmatrix} c_a \\ c_b \end{bmatrix} = E \begin{bmatrix} c_a \\ c_b \end{bmatrix}. \tag{5}$$

The electron transfer in a QCA cell is driven by the interaction with a neighboring molecule. Figure 4 illustrates

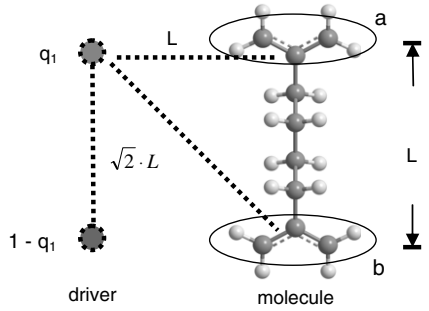

Figure 4. Coulomb interaction between neighboring molecules. The mobile charge can move from one dot to the other within the molecule, but cannot move outside the molecule. The charge population of each dot varies from 0 to 1. The upper dot and the bottom dot of the target molecule are denoted as a and b, respectively.

the Coulomb interaction between two neighboring molecules. The molecule on the left we take to be the driver, and describe it using two point charges. The molecule on the right will be described with the two-state approximation. The distance between the two redox centers (dots) of the molecule is L. For simplicity we take the distance between two neighboring molecules to be L also, such that the four dots of two of the neighboring molecules form a square. We can describe the intermolecular interaction by a simple electrostatic calculation. A fuller description of cell–cell interactions would employ a chain of molecular cells driven by a single driver, thereby including molecule–molecule interactions in a self-consistent way. For simple molecules, this has been done [6]. For characterizing the intrinsic bistability of larger molecules, a simple electrostatic model of the driver is sufficient.

We now derive the relation between the polarizations of two neighboring molecules.

Suppose each molecule has one mobile charge. We define the polarization P of a double-dot molecule as shown in figure 4:

$$P = \frac{q_a - q_b}{q_a + q_b} \tag{6}$$

where q_a and q_b represent the charge population of the upper dot and the bottom dot. For a double-dot QCA molecule which contains one mobile charge, $q_a + q_b = 1$. Thus we have

$$P = q_a - q_b. \tag{7}$$

We denote the driver's charge configuration as q_1 distributed in dot 1 and $1 - q_1$ in dot 2, while q_1 varies from 0 to 1. According to the above definition of polarization, the polarization of the driver is $P_1 = q_1 - (1 - q_1) = 2q_1 - 1$. We wish to calculate the ground state polarization P_2 of the target molecule produced by interaction with the driver molecule.

We can represent the target molecule's diabatic energies as

$$\begin{aligned} H_{aa} &= \frac{1}{4\pi\varepsilon_0}\frac{q_1 e}{L} - \frac{1}{4\pi\varepsilon_0}\frac{(1-q_1)e}{\sqrt{2}L} \\ H_{bb} &= \frac{1}{4\pi\varepsilon_0}\frac{q_1 e}{\sqrt{2}L} - \frac{1}{4\pi\varepsilon_0}\frac{(1-q_1)e}{L} \end{aligned} \tag{8}$$

where e is the unit charge and ε_0 is the permittivity of the vacuum. (The molecule–molecule interaction is through the vacuum.) By solving the secular determinant equation (2) we obtain

$$E = \frac{(H_{aa} + H_{bb}) \pm \sqrt{(H_{aa} - H_{bb})^2 + 4\gamma^2}}{2} \tag{9}$$

and

$$\begin{aligned} c_a^2 &= \frac{\gamma^2}{\gamma^2 + (E - H_{aa})^2} \\ c_b^2 &= \frac{(E - H_{aa})^2}{\gamma^2 + (E - H_{aa})^2}. \end{aligned} \tag{10}$$

With the coefficient c_a and c_b we can represent the polarization of the target double-dot molecule according to (7)

$$P_2 = c_a^2(+1) + c_b^2(-1) = 2c_a^2 - 1 \qquad (\text{since } c_a^2 + c_b^2 = 1). \tag{11}$$

Inserting (10) into (11) we have

$$P_2 = \frac{2\gamma^2}{\gamma^2 + (E - H_{aa})^2} - 1. \tag{12}$$

From (9) we obtain

$$P_2 = \frac{2\gamma^2}{\gamma^2 + \left[\frac{(H_{aa}+H_{bb}) \pm \sqrt{(H_{aa}-H_{bb})^2+4\gamma^2}}{2} - H_{aa}\right]^2} - 1 \tag{13}$$

and finally we insert (8) into (13) and represent the driver's polarization as $P_1 = 2q_1 - 1$, yielding

$$\begin{aligned} P_2 = {} & \{2\gamma^2 L^2\} \\ & \times \left\{ \gamma^2 L^2 + \left\{ \frac{e^2}{4\pi\varepsilon_0}\left(\frac{2-\sqrt{2}}{4}\right) P_1 \right.\right. \\ & \left.\left. + \sqrt{\left(\frac{e^2}{4\pi\varepsilon_0}\right)^2 \left(\frac{2-\sqrt{2}}{4}\right)^2 P_1^2 + \gamma^2 L^2} \right\}^2 \right\}^{-1} - 1. \end{aligned} \tag{14}$$

We can rewrite this in terms of a dimensionless quantity which characterizes the nonlinearity:

$$P_2 = \frac{2}{1 + \left\{\beta P_1 + \sqrt{\beta^2 P_1^2 + 1}\right\}^2} - 1 \tag{15}$$

where

$$\beta \equiv \frac{e^2}{4\pi\varepsilon_0}\left(\frac{2-\sqrt{2}}{4}\right)(\gamma L)^{-1} \approx \frac{0.2109\,(\text{eV nm})}{\gamma L}. \tag{16}$$

Differentiating to find the slope of the cell–cell response function at the origin results in the simple relation

$$\left.\frac{\mathrm{d}P_2}{\mathrm{d}P_1}\right|_{P_1=0} = -\beta. \tag{17}$$

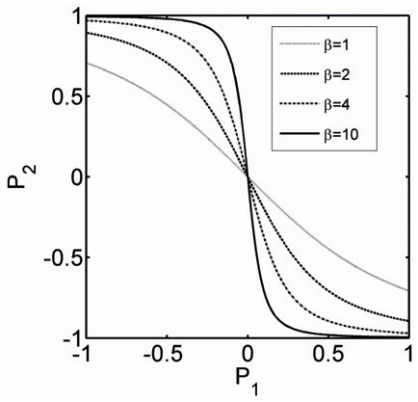

Figure 5. The cell–cell response functions obtained from equation (15) for different values of β.

The saturation value of P_2 ($P_1 = -1$) can also be determined from just β:

$$P^{\text{sat}} = \frac{2}{1 + \left(\sqrt{\beta^2 + 1} - \beta\right)^2} - 1. \tag{18}$$

Equation (15) is an important result. It relates the polarization of the target molecule with that of the driver molecule, so that, given the polarization of the driver molecule, the polarization of the target molecule is determined by the molecular structure parameters γ and L (through the value of β). The matrix element γ is an electronic structure parameter which describes the ease with which the mobile charge may tunnel from one redox center to the other—a larger value of γ means tunneling is easier. It can be measured via spectroscopic experiments including absorption [21, 22], EPR [23], and ultraviolet photoelectron spectroscopy (UPS) [24], or calculated using various quantum chemistry techniques [25]. The molecular structure parameter L is simply the geometric distance between the two redox centers which form the dots, and can also be obtained either experimentally or from a theoretical calculation.

Equation (15) relates key features of molecular structure (the distance L and ET matrix element γ) to QCA functionality as expressed in the cell–cell response function P_2 (P_1). This response function could in principle be calculated from a complete *ab initio* quantum chemistry model, as we do below, but that is often prohibitively complex. Equation (15) allows us to obtain a good approximation to the response function, provided we can obtain, either experimentally or theoretically, good values for L and γ.

More importantly, equation (15) provides a tool to guide molecular design. The length L results from the choice of the redox center which forms the dot and the length of the bridge which connects them. The ET matrix element γ is determined by the electronic structure of the redox center, the nature of the bridge (e.g. saturated versus unsaturated) and the interaction between them [26]. Both parameters provide many degrees of freedom with which we can design molecules that satisfy the fundamental requirements of QCA cells.

The nonlinearity of the cell–cell response function key to QCA operation is determined in this simple model entirely by the value of β, the slope at the origin. Good QCA switching is obtained for $\beta > 1$. To meet this requirement, we need a molecule which satisfies $\gamma L < 0.21$ eV nm. For example, a molecule with a distance of 1 nm between its two redox centers must have a matrix element γ less than 0.21 eV. Figure 5 demonstrates the dependence of the cell–cell response function on the values of β.

In designing molecular QCA we want β to be larger than one, which means we want the ET matrix element γ as small as possible and L as small as possible. In fact, the design space for L is limited to the region between 0.1 and 2 nm. The lower limit is the size of a single atom; the upper limit is because we need the interaction energy between cells to be large compared to $k_B T$. Therefore most of the design goes into choosing γ, which can be varied over many orders of magnitude (reflected in the large variation in ET rates). Ultimately, the desirability of rapid QCA switching rates will impose a practical lower limit on γ, but this will not be addressed here.

3. Application

3.1. Hydrogen molecular cation H_2^+

In this section and the following sections we calculate the molecule's energy levels and charge distribution under the influence of a charge driver with the unrestricted Hartree–Fock (UHF) method and the state average complete active space self-consistent field (CASSCF) method. The hydrogen molecular cation H_2^+ provides the simplest, though unrealistic, model of molecular QCA switching. We use H_2^+ because it has a simple electronic structure which can be easily solved by various methods. For the state average CASSCF calculation, the active space includes the four lowest orbitals and only one electron, specified as CASSCF(1, 4). The charge driver, which mimics a nearby molecule, is constructed from two point charges with varying strengths as shown in figure 4.

Since H_2^+ has only one electron, electron exchange and correlation effects are absent and the single-determinant HF model reduces to a one-electron calculation which accurately describes the ET process of the molecule. We then compare the *ab initio* results with equation (15) derived in section 2. This simple molecule serves as the first computational test of our theoretical model. All *ab initio* calculations of the H_2^+ system were performed in Gaussian03 [27] with an aug-cc-p VTZ basis set. For HF calculations we use Koopmans' theorem and approximate the energy levels of the ground and excited states of H_2^+ by the energies of the HOMO and HOMO-1 orbitals of the neutral H_2 triplet state. Since the charge configuration is a ground state property, the response function can be calculated for the cation directly.

To investigate the effect of molecular structure on the switching behavior of QCA cells, we examine H_2^+ with various distances between the two hydrogen atoms. Hereafter we denote H_2^+ as the H_2 cation with an H–H distance of 1.058 Å—the equilibrium geometry—and we denote as H_2^{+*}, H_2^{+**} and H_2^{+***} the H–H^+ pairs with nuclear distances of 2.5 Å, 4 Å

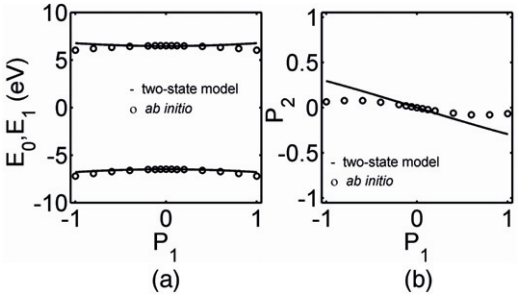

Figure 6. Switching of H_2^+ in its equilibrium structure. (a) Energy diagram. (b) Cell–cell response function. It is worth noting that HF and CASSCF calculations give identical results for H_2^+. Since there is only one electron in the system, a multiple-determinant wavefunction does not improve the computational result. Therefore, we present only the CASSCF result and label it as '*ab initio.*'.

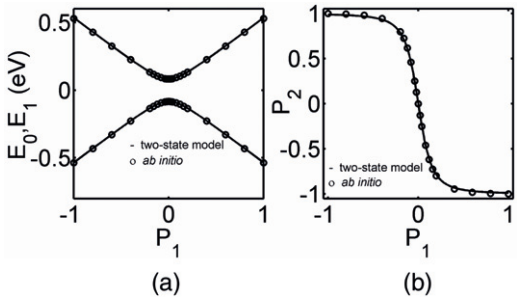

Figure 7. Switching of H_2^+ with an H–H distance of 4 Å. (a) Energy diagram. (b) Cell–cell response function.

and 10 Å, respectively. We do this for two reasons. First, by varying the inter-well distance of the same 'double-well' system we can gain information on how a molecular QCA cell's electronic structure relates to its geometric structure. Second, the comparison of cell-switching behavior obtained from *ab initio* calculations and the two-state model enables us to check the validity of equation (15).

The H_2^+ molecule does not perform well as a QCA cell. At the equilibrium geometry (H–H bond length of 1.058 Å), H_2^+ has a very stable ground state because the bonding orbital lies between two hydrogen atoms, and the first excited state is far above the ground state (the excitation energy is above 10 eV). Thus for the equilibrium structure of H_2^+ there are no well-defined bistable states capable of encoding binary information. Figure 6 shows the energy diagram and the cell–cell response function of H_2^+ as a function of the neighboring driver's polarization. The figure shows results from both the CASSCF method and the two-state model (equations (9) and (15)). The ET matrix element γ for the two-state model is determined by the energy splitting at $P_1 = 0$ from the CASSCF calculation. Because H_2^+ has a large ET matrix element γ (>5 eV), evidenced by the large energy gap between the ground state and the excited state in figure 6(a), the interaction between the ground state and the first excited state is rather weak. The local electric field is not strong enough to induce charge localization, which can be seen from figure 6(b). Even with the driver fully polarized, H_2^+ has a weak polarization of less than 0.1.

Figure 6 also shows obvious discrepancies between the *ab initio* calculation and equation (15). This is unsurprising since equation (15) is based on the TSA which assumes two well-defined and localized '0' and '1' states. When two H atoms approach each other and form an H_2^+ cation at its equilibrium bond length, two localized atomic orbitals form a pair of bonding and anti-bonding orbitals which delocalize between the two atoms. This is essentially the meaning of a chemical bond pointed out by Heitler and London 80 years ago [28]. This suggests that very strong interaction between two quantum dots in a QCA molecule will result in the loss of bistability and thus the ability to encode binary information. If the two dots merge to form one dot, then QCA cannot work.

A modified H_2^+ molecule with a larger inter-atomic distance starts to show the bistability required for QCA functionality. It is well known that the electronic matrix element decreases exponentially as the distance between the redox centers increases [15]. Since H_2^+ serves only as a model molecule in this work, we can set the bond length at any value convenient for investigating the structure–property relation of QCA cells. Figure 7 shows the results for H_2^+ with a bond length of 4 Å. Figure 7(a) plots the energy levels of the ground and first excited states. With a large distance between atoms, the energy gap is greatly decreased. As the driver polarization increases, the energy of the two lowest-lying states becomes linearly dependent on driver polarization, suggesting that the charge configuration of the driver strongly favors one state over the other. The response function in figure 7(b) is consistent with this, showing that the binary state of the molecule can be switched by its neighbor.

Figure 7 also demonstrates close agreement between the *ab initio* calculation (dots) and the two-state model (solid line) given by equation (15) with β determined by the chosen L and the calculated energy gap at $P_1 = 0$ using equation (4b). This agreement shows there is no strong interaction between two well-separated H atoms, so that the two atomic orbitals provide two well-defined localized states. Thus for this system the two-state approximation does an excellent job of describing the driver-induced electron transfer, which is critical for QCA operation. Although the H_2^+ system has only one electron, making the *ab initio* calculations rather simple, the good agreement in figure 7 demonstrates that the interaction between QCA cells is essentially electrostatic and can be captured by the two structural parameters of our model.

The effect of different structural parameters can be seen by comparing figures 6 and 7. The cell–cell response function in figure 6(b) differs from that in figure 7(b) due to the differing energy gaps between the two low-lying states seen in figures 6(a) and 7(a). Since the electronic matrix element γ decreases exponentially with the distance, the product γL is much smaller for a larger L, so that the molecule becomes more polarized under a local field perturbation. As can be seen in figure 7(b), the polarization of the target molecule nearly reaches unity when the driver is fully polarized. It is this fully polarized character that provides a well-defined binary bit.

Further increase of the H–H distance confirms this trend in the structure–property relation. Figure 8 shows the energy

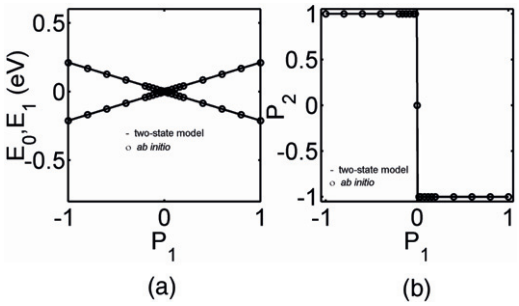

Figure 8. Switching of H_2^+ with an H–H distance of 10 Å. (a) Energy diagram. (b) Cell–cell response function.

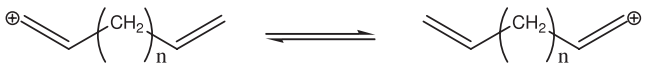

Chart 1. Alkyl-diene molecule cation.

Table 1. Parameters of H_2^+ at different H–H distances.

	H_2^+	H_2^{+**}	H_2^{+**}	H_2^{+***}
L_{HH} (nm)	0.1058	0.25	0.4	1
γ (eV)	6.5	0.84	0.083	0.0001
γL_{HH} (eV nm)	0.6877	0.21	0.0332	0.0001
β	0.31	1	6.4	2109

diagram (figure 8(a)) and the cell–cell response function (figure 8(b)) for an H–H distance of 10 Å. At this large H–H distance, there is essentially no interaction between the two atomic orbitals, corresponding to an ET matrix element γ of almost zero (figure 8(a)). The response function demonstrates abrupt cell-switching upon driver polarization. Even a small driver signal can induce a large polarization in the target molecule.

Table 1 lists the values of structural parameters γ and L for different H–H distances. As the H–H distance increases, the ET matrix element γ decays exponentially, and as a result the slope of the response function at the origin, β, increases significantly. For the H_2^+ molecule in the equilibrium structure, the slope is less than 1, resulting in a sub-linear response with no 'signal gain' (figure 6). At an H–H distance of 2.5 Å, the β parameter has a value of 1, yielding output polarization equal to that of the input driver. Further increases of the H–H distance gives larger values of β, yielding the 'signal gain' mentioned above.

3.2. Alkyl-diene cation

The second model system we investigate is the alkyl-diene cation, shown in chart 1, which consists of two ethylene groups connected by an alkyl bridge. In chart 1 n is the number of methylene groups, and in this work we study the system for $n = 3$, 5, 7 and 9. In the molecular cation one ethylene group is neutral and the other is cationic. The unpaired electron can occupy the π bond of either ethylene group with little change to the molecular geometry. The possibility of using π systems for a QCA model has been explored in previous work [6].

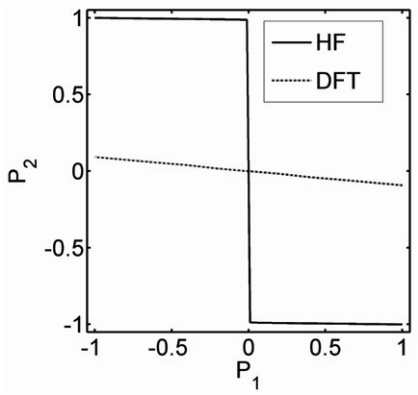

Figure 9. The cell–cell response function of 1, 10-undecadiene cation calculated at the UHF and DFT levels when driven by the charge driver shown in figure 4.

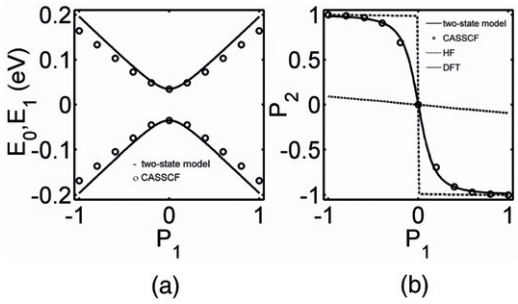

Figure 10. Switching of the 1,10-undecadiene cation. (a) Energy diagram. (b) Cell–cell response function. The results shown are obtained from the state average CASSCF method (dots) and the two-state model (solid line), as well as from the single-determinant UHF (dotted line) and DFT (dashed line) methods.

Unlike H_2^+, the diene cation is a multi-electron system, which a single-determinant wavefunction cannot fully describe because the electron correlation effects need to be taken into account. Among these single-determinant *ab initio* techniques, it is well known that the UHF method overestimates charge localization and density functional theory (DFT) methods underestimates it [16–19]. The UHF method overestimates charge localization due to its neglect of electron correlation effects, while the overestimation of the DFT method is attributed to the exchange potential defined in hybrid functionals [17]. In figure 9 we present the UHF- and DFT-calculated response functions for a 1,10-undecadiene ($n = 7$) cation driven by the charge driver shown in figure 4. The UHF calculation is performed with a 6-31G* basis set and the DFT calculation with the B3LYP algorithm and 6-31G* basis set. From figure 9 one can see that the UHF result demonstrates very strong nonlinearity in the response curve. Even a small driver polarization induces essentially complete polarization in the target molecule. In contrast, the DFT result is nearly linear. The discrepancy between these two methods suggests that a higher-level treatment—beyond that of a single-determinant wavefunction—is needed to accurately describe multi-electron systems like the alkyl-diene cation.

We here employ a multi-determinant method, CASSCF, to describe this model QCA system. It is believed that

Table 2. Ethylene–ethylene distance and coupling in the diene cation series.

	E–$(CH_2)_3$–E	E–$(CH_2)_5$–E	E–$(CH_2)_7$–E	E–$(CH_2)_9$–E
L_{AA} (nm)	0.5474	0.8225	1.095	1.357
γ (eV)	0.52	0.1276	0.0351	0.0119
γL_{MM} (eV nm)	0.285	0.105	0.0384	0.0161
β	0.74	2.01	5.49	13.10

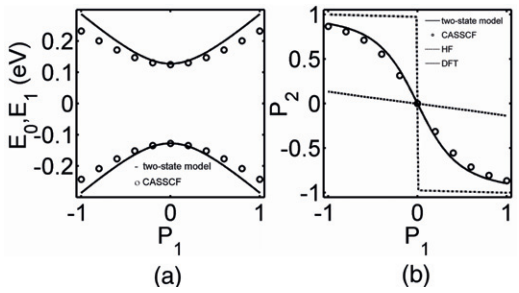

Figure 11. Switching of the 1,8-nonadiene cation. (a) Energy diagram. (b) Cell–cell response function. The results shown are obtained from the state average CASSCF method (dots) and the two-state model (solid line), as well as from the single-determinant UHF (dotted line) and DFT (dashed line) methods.

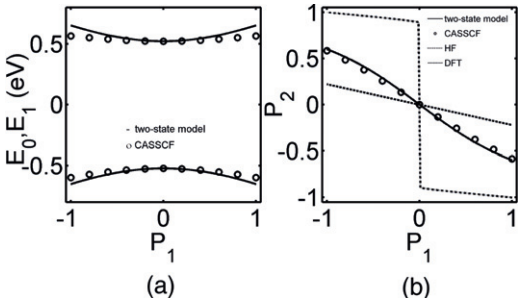

Figure 12. Switching of the 1,6-heptadiene cation. (a) Energy diagram. (b) Cell–cell response function. The results shown are obtained from the state average CASSCF method (dots) and the two-state model (solid line), as well as from the single-determinant UHF (dotted line) and DFT (dashed line) methods.

the CASSCF method is the most reliable for describing the charge distribution of a mixed-valence complex [29]. The alkyl-diene cation is a small enough system that use of the CASSCF method is practical. Figure 10 shows the calculated energy diagram and cell–cell response function for the 1,10-undecadiene cation obtained with a state average CASSCF method [29]. The active space is composed of all three π electrons in four π orbitals, referred to as CAS(3, 4). The advantage of CASSCF is that it calculates both the ground state and the excited states, and the state average technique allows mixing those states in solving the secular equation to determine the adiabatic eigenstates. Since the state average CASSCF takes into account both ground and excited states, its results are closer to the exact eigenstates than those of UHF. Figure 10(b) shows the cell–cell response function. As the driver's polarization changes, the target molecule switches smoothly, although it saturates quickly.

Figure 10 also shows the results calculated from the two-state model, using equation (9) to obtain the energy diagram shown in figure 10(a) , and equation (15) to obtain the cell–cell response function shown in figure 10(b). The ET matrix element γ for the two-state model is determined by the energy splitting at $P_1 = 0$ from the CASSCF calculation. For the alkyl-diene cation, this simple two-state model is in remarkably good agreement with the high level state average CASSCF calculation. It must be pointed out that, for this multi-electron system, the single-determinant UHF method fails to give the correct response function. The multi-configuration CASSCF plus state average technique is needed to obtain the correct switching behavior from an *ab initio* approach.

For realistic QCA candidate molecules, which may well include transition metals and other ligands, multi-configuration calculations become very expensive. The simple two-state approximation of equations (9) and (15) does a remarkable job of generating both the energy diagram and response function. The two-state model ignores the details of the molecular electronic structure but captures (a) the electrostatics that provide the driving force in QCA switching and (b) the essential feature of electron transfer through knowledge of one number—the ET matrix element γ. (The model must rely on another source for the value of γ, either experimental or theoretical.) Its success suggests that for these purposes we can adequately describe electron transfer in mixed-valence complexes as an electrostatically driven one-electron problem in which other electrons can be considered frozen in their orbitals.

As with the previously described molecular hydrogen cation, as the distance between redox centers in the diene system diminishes, clear separation of 'dots' deteriorates and QCA switching degrades. We compute the energy diagram and response function for 1,8-nonadiene ($n = 5$) cations and 1,6-heptadiene ($n = 3$) cations, shown in figures 11 and 12. The properties of these two diene cations with shorter bridges are similar to those of the 1,10-undecadiene cation shown in figure 10. As the bridge becomes shorter, the energy gap increases and molecules gradually lose bistability and switchability. For each of these diene cations, the molecular energies and polarization response given by the simple model equations (9) and (15) are in good agreement with state average CASSCF calculations, while the UHF and DFT computations overestimate or underestimate charge localization, respectively. The ET matrix element γ for the two-state model is again determined by the energy splitting at $P_1 = 0$ from the CASSCF calculation.

Structural parameters γ and L for the diene cation series are computed and listed in table 2. The dot–dot distance L is taken to be the distance between the centers of the double bonds. A trend similar to that of the $H–H^+$ system can be seen as the dot–dot distance increases: the ET matrix element decays exponentially, resulting in an increase in the slope of

Table 3. Metal–metal distances and ET matrix elements in the Fc–*n*–Fc series.

	Fc–1–Fc	Fc–2–Fc	Fc–3–Fc	Fc–4–Fc	Fc–5–Fc
L_{MM} (nm)	0.703	0.921	1.154	1.387	1.629
γ^{exp}(eV)[a]	0.061	0.053	0.048	0.035	0.028
γ^{cal} (eV)	0.100	0.070	0.050	0.0345	0.024
γL_{MM} (eV nm)^{exp}	0.0429	0.0488	0.0554	0.0485	0.0456
γL_{MM}(eV nm)^{cal}	0.0703	0.0645	0.0577	0.0479	0.0391
β^{exp}	4.9	4.3	3.8	4.3	4.6
β^{cal}	3.0	3.3	3.7	4.4	5.4

[a] Experimental values from [30].

the response function at the origin, β. The rate of decay with dot–dot distance will be discussed in the following section.

The above analysis of the H–H$^+$ and diene cation systems of various lengths suggest that the two-state model may provide a reliable means for correlating the molecular structure–property relation in complicated mixed-valence complexes for which more accurate *ab initio* techniques are intractable.

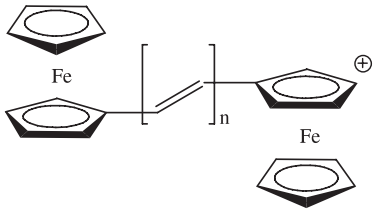

Chart 2. Mixed-valence diferrocenylpolyenes.

3.3. Mixed-valence diferrocenylpolyenes

One class of QCA candidate molecules which has been explored experimentally is comprised of mixed-valence diferrocenyl compounds [30], which contain two ferrocenyl groups (Fc) acting as quantum dots. It is known that Fc is usually stable when the iron is in the formal oxidation states of 2+ and 3+, enabling the mobile charge to move between the two Fc groups, thus providing two stable charge configurations [31, 32]. Furthermore, it has been possible to examine the mixed-valence behavior of such compounds as a function of distance between two interacting Fc groups, as a function of the nature of the bridge between them, and as a function of their relative orientations.

Here we investigate the switching behavior of mixed-valence diferrocenylpolyene compounds when used as a QCA cell. We are interested in this series of compounds for two reasons. First, there exists a large body of experimental data for diferrocenylpolyenes and their derivatives. The ET matrix elements have been explored with spectroscopic methods [30, 33, 34]; the metal–metal distance has been measured with x-ray crystallography [35, 36] and estimated using a PC model [30]; and the effect of bridge substitution has been investigated [37]. Second, because of the complexity of the electronic structure of transition metal complexes, reliable quantum chemical modeling is difficult. Single-determinant UHF and DFT methods fail to treat the multi-electron system as discussed in section 3.2, making it difficult to obtain reliable results for the more complicated diferrocenylpolyene. The more reliable, multiple-determinant state average CASSCF calculation is extremely difficult for this type of compound. In this situation, the molecular QCA structure–property relation derived from equation (15) is useful for investigating the switching behavior of the molecules, and in evaluating the feasibility of using these molecules as QCA cells.

To understand the structure–property relation of molecules with the two-state model described above, we need to know two important structure parameters: the ET matrix element γ and the dot–dot distance L. In the preceding sections we were able to obtain γ from the energy splitting at zero driver using a CASSCF calculation. Because for a system of this size such a calculation is unavailable, we here use Koopmans' theorem [38] to calculate the matrix element γ. For intramolecular ET between the Fc cation and the neutral Fc, γ can be approximated by one-half of the difference in molecular orbital (MO) energy between the highest occupied molecular orbital (HOMO) and the second highest occupied molecular orbital (HOMO-1) of the neutral system. According to the one-electron Koopmans' theorem, the ionization potential of HOMO and HOMO-1 can be expressed as the SCF energies, i.e.

$$\begin{aligned} I_{HOMO} &= -\varepsilon_{HOMO} \\ I_{HOMO-1} &= -\varepsilon_{HOMO-1}. \end{aligned} \tag{19}$$

Therefore, the transition energy from HOMO-1 to HOMO can be expressed as the MO energy splitting factor, Δ:

$$\Delta = 2\gamma = I_{HOMO-1} - I_{HOMO} = \varepsilon_{HOMO} - \varepsilon_{HOMO-1}. \tag{20}$$

The above calculation has been performed employing a DFT B3LYP method and the 6-31G basis set. In the above discussion we have shown that DFT usually underestimates charge localization for mixed-valence complexes and thus is unsuitable for computing the charge distribution of this type of molecule. However, we are here computing the MO energy, for which DFT methods have proven reliable, as can been seen from table 3. This is a single point calculation for the symmetric nuclear geometry, at which the mobile charge is intrinsically delocalized between the two redox centers. In the following discussion, these compounds of general form Fc(CH=CH)$_n$Fc containing two ferrocene units linked by n conjugated double bonds, as shown in chart 2, will be denoted Fc–*n*–Fc.

Table 3 lists the calculated ET matrix element γ together with experimentally obtained values [30]. Although

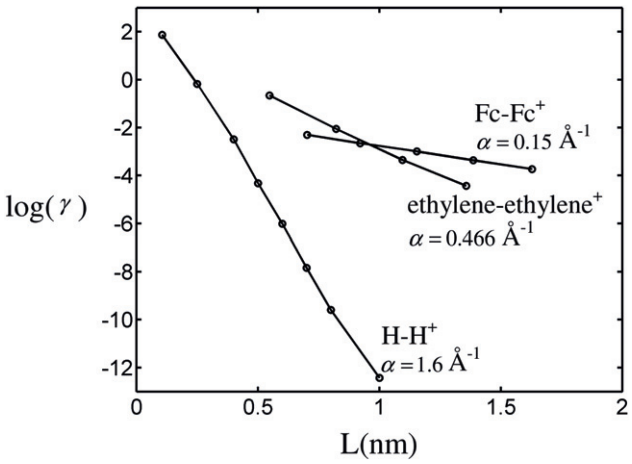

Figure 13. Decay of the ET matrix element (log scale) with distance.

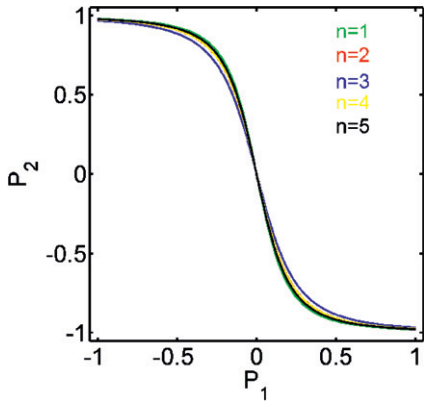

Figure 14. The cell–cell response function of Fc–*n*–Fc calculated with equation (15).
(This figure is in colour only in the electronic version)

Koopmans' theorem is a simplified approximation, the calculated values qualitatively agree with experimental results. For $n = 3, 4, 5$, they agree very closely, suggesting that Koopmans' theorem could be used to evaluate the ET matrix element of complicated mixed-valence complexes including transitional metals, for which direct calculation of molecular charge configuration is difficult. Table 3 also lists the metal–metal distance obtained from PC model simulation [30]. With these two structural factors, we can estimate the molecule's switching behavior when used as a QCA cell.

It is well known that the ET matrix element γ decays exponentially with dot–dot distance [15]. The plot of $\log(\gamma)$ versus L for H–H$^+$, ethylene–ethylene$^+$ and Fc–Fc$^+$ are given in figure 13. For all three systems, the plot confirms the exponential decay of the ET matrix element with distance. The H–H$^+$ system has the fastest decay, with a slope of 1.6 Å^{-1}. This is expected since the ET between two H atoms is a through-space transfer. This decay rate is faster than those of the through-bond transfer of the ethylene–ethylene and Fc–Fc systems. Compared with alkyl-diene cation compounds, diferrocenylpolyene has a conjugated double-bond bridge as opposed to a saturated alkyl bridge. The conjugated bridge gives the two Fc groups a stronger, less distance-dependent interaction resulting in a smaller decay rate. For the diferrocenylpolyene system, the decay slope is 0.15 Å^{-1}, corresponding to a decrease of a factor of 2 for each 4.6 Å. Compared with the experimental value [30] of 0.113 Å^{-1}, the decay rate predicted from Koopmans' theorem is satisfactory.

Finally, with the structural factors γ and L, we calculate the predicted cell–cell response function of Fc–*n*–Fc (figure 14). Experiments have not yet been able to probe this response function directly, due to the challenge of making nearby single-molecule measurements. Figure 14 shows the diferrocenylpolyene molecule has a strongly nonlinear response function when used as a QCA cell. The derivative of P_2 with respect to P_1 at the origin, β, is about 4, which supports signal gain in the information transfer. When driven by a fully polarized neighboring molecule, the target molecule demonstrates a maximum polarization above 0.9, giving two well-defined localized states capable of encoding binary information. From figure 14 we also see that, although the ET matrix decays exponentially with dot–dot distance, the diferrocenylpolyene series demonstrates very similar response functions for various bridge lengths, which can also be seen from table 3. This is due to the fact that the decay exponent α is very small compared with the decay exponents of the H–H$^+$ and ethylene–ethylene systems so β varies more slowly with the distance between dots.

4. Conclusion

We have presented a theoretical model to correlate the molecular QCA structure–property relationship. This structure–property relationship provides a simple yet reliable tool to examine the bistability of candidate molecules, which is a fundamental requirement for QCA cells. Equation (15) provides a connection between two structural parameters, the dot–dot distance L and the ET matrix element γ. Both parameters can be measured by well-established experimental techniques, and can be obtained via first-principle computation. In the case of the complicated mixed-valence complexes, although the accurate state-of-the-art quantum chemistry methods may be computationally intractable, a single-point DFT calculation based on Koopmans' theorem still provides a reasonably accurate value for γ. Thus the model developed in this work can be easily applied to various molecular QCA candidates.

We test this theory on two model molecules. The hydrogen molecular cation H–H$^+$ is the simplest possible model, having only one electron. The available quantum chemistry techniques from the single-determinant UHF (which here is even simpler) to the sophisticated multi-configuration state average CASSCF present the exact solutions, and those solutions are in good agreement with our model. Varying the distance between H atoms varies the couplings between the two states. For both weak and strong coupling, our model performs reliably, so long as it makes sense to distinguish two localized states. For the more complicated alkyl-diene cation, the single-determinant UHF and DFT methods overestimate or underestimate the charge localization, and thus fail to describe the switching

behavior of the molecule. We compare our model with the results obtained from the more reliable state average CASSCF calculation. These studies suggest that our model still produces reliable solutions for the charge configuration of a multi-electron system in a field-induced ET process.

Finally, we apply our model to more realistic QCA candidate molecules, exploring the switching behavior of mixed-valence diferrocenylpolyenes. Without a reliable first-principle technique, we estimate the electronic matrix elements using Koopmans' theorem and model the molecule's switching behaviors as a QCA cell. The mixed-valence diferrocenylpolyenes show well-defined localization and nonlinear bistable response. We suggest the approach developed here can provide a simple and relatively accurate way of determining the bistability of candidate molecules for use in QCA.

We have limited our focus here in three respects that merit highlighting: firstly, though ultimately four- and six-dot QCA cells will be extremely useful, the basic elements of QCA switching can be examined with a simple two-dot cell [6, 11, 13]. The polarization of two-dot molecular QCA cells can be related straightforwardly to a well-known property—the molecule's dipole moment. This can be measured in bulk samples and computed using quantum chemistry techniques. For four-dot cells the corresponding quantity is the quadrupole moment. For complex circuits and systems requiring power gain a three- or six-dot clocked cell is important [39, 40]. Here we have focused on the fundamental properties of bistability and switching that can be well characterized in the simpler two-dot system.

Secondly, we have not addressed here the several other requirements that a practical QCA system must exhibit. These include such things as functionalization for surface attachment and orientation, isolation of mixed-valence states, control or elimination of counter-ion effects, input and output of molecular signals, and implementation of field-driven clocking. We have focused on the most basic aspects of encoding and processing binary information in molecular states—bistability and switching.

Thirdly, the relaxation of nuclear degrees of freedom associated with electron transfer has not been considered here. It is true that studying mixed-valence complexes in solution has led to considerable attention to this 'reorganization energy' which shifts the electronic states due to the nuclear relaxation. In this context the Robin Day classification scheme is well known. As discussed at length elsewhere [6], for QCA the key question is electronic localization (and bistability) with frozen nuclear positions. Ligand relaxation complicates matters, to be sure, especially considering the different timescales involved. But for anticipated high-speed operation of molecular QCA we need bistability in the electronic degrees of freedom independent of nuclear relaxation. The problem of ligand relaxation locking in a bit will need to be considered in due course.

References

[1] Lent C S, Tougaw P D, Porod W and Bernstein G H 1993 *Nanotechnology* **4** 49

[2] Lent C S and Tougaw P D 1993 *J. Appl. Phys.* **74** 6227

[3] Orlov A O, Amlani I, Bernstein G H, Lent C S and Snider G L 1997 *Science* **277** 928

[4] Amlani I, Orlov A O, Toth G, Bernstein G H, Lent C S and Snider G L 1999 *Science* **284** 289

[5] Orlov A O, Amlani I, Toth G, Lent C S, Bernstein G H and Snider G L 1999 *Appl. Phys. Lett.* **74** 2875

[6] Lent C S, Isaksen B and Lieberman M 2003 *J. Am. Chem. Soc.* **125** 1056

[7] Lent C S and Isaksen B 2003 *IEEE Trans. Electron Devices* **50** 1890

[8] Lent C S 2000 *Science* **288** 1597

[9] Lu Y and Lent C S 2005 *J. Comput. Electron.* **4** 115

[10] Lent C S, Liu M and Lu Y 2006 *Nanotechnology* **17** 4240

[11] Qi H, Sharma S, Li Z, Snider G L, Orlov A O, Lent C S and Fehlner T P 2003 *J. Am. Chem. Soc.* **125** 15250

[12] Jiao J, Long G J, Grandjean F, Beatty A M and Fehlner T P 2003 *J. Am. Chem. Soc.* **125** 7522

[13] Qi H, Gupta A, Noll B C, Snider G L, Lu Y, Lent C S and Fehlner T P 2005 *J. Am. Chem. Soc.* **127** 15218

[14] Jiao J, Long G J, Rebbouh L, Grandjean F, Beatty A M and Fehlner T P 2005 *J. Am. Chem. Soc.* **127** 17819

[15] Newton M D and Cave R J 1997 *Mol. Electron.* **73**

[16] Tajkhorshid E and Suhai S 1999 *J. Phys. Chem.* B **103** 5581

[17] Cabrero J, Calzado C J, Maynau D, Caballol R and Malrieu J P 2002 *J. Phys. Chem.* A **106** 8146

[18] Braun-Sand S B and Wiest O 2003 *J. Phys. Chem.* A **107** 285

[19] Yokogawa D, Sato H, Nakao Y and Sakaki S 2007 *Inorg. Chem.* **46** 1966

[20] Yamamoto N, Vreven T, Robb M A, Frisch M J and Schlegel H B 1996 *Chem. Phys. Lett.* **250** 373

[21] Hush N S 1967 *Prog. Inorg. Chem.* **8** 391

[22] Hush N S 1968 *Electrochim. Acta.* **13** 1005

[23] Bailey S E, Zint J I and Nelson S F 2003 *J. Am. Chem. Soc.* **125** 5939

[24] Coropceanu V, Gruhn N E, Barlow S, Lambert C, Durivage J C, Bill T G, Nöll G, Marder S R and Brédas J-L 2004 *J. Am. Chem. Soc.* **126** 2727

[25] Newton M D 1991 *Chem. Rev.* **91** 767

[26] Kilså K, Kajanus J, Macpherson A N, Mårtensson J and Albinsson B 2001 *J. Am. Chem. Soc.* **123** 3069

[27] Frisch M J *et al* 2003 *Gaussian 03, Revision A.1* (Pittsburgh, PA: Gaussian, Inc.)

[28] McQuarrie D A 1983 *Quantum Chemistry* (London: Oxford University Press)

[29] Malmqvist P-A and Roos B O 1989 *Chem. Phys. Lett.* **155** 189

[30] Ribou A-C, Launay J-P, Sachtleben M L, Li H and Spangler C W 1996 *Inorg. Chem.* **35** 3735

[31] Dong T-Y, Chang L-S, Tseng I-M and Huang S-J 2004 *Langmuir* **20** 4471

[32] Dong T-Y, Shih H-W and Chang L-S 2004 *Langmuir* **20** 9340

[33] Delgadopena F, Talham D R and Cowan D O 1983 *J. Org. Chem.* **253** C43

[34] Chen Y J, Pan D-S, Chiu C-F, Su J-X, Lin S J and Kwan K S 2000 *Inorg. Chem.* **39** 953

[35] Amer S I, Sadler G, Henry P M, Ferguson G and Ruhl B L 1985 *Inorg. Chem.* **24** 1517

[36] Dong T-Y, Ke T-J, Peng S-M and Yeh S-K 1989 *Inorg. Chem.* **28** 2103

[37] Justin Thomas K R, Lin J T and Wen Y S 2000 *Organometallics* **19** 1008

[38] Koopmans T 1934 *Physica* **1** 104

[39] Amlani I, Orlov A O, Snider G L, Lent C S and Bernstein G H 1998 *Appl. Phys. Lett.* **72** 2179

[40] Timler J and Lent C S 2002 *J. Appl. Phys.* **91** 823